Nanoscale

PAPER

View Article Online
View Journal | View Issue

Open Access Article. Published on 06 May 2016. Downloaded on 12/5/2025 12:51:01 PM.
This article is licensed under a Creative Commons Attribution 3.0 Unported Licence.

Cite this: *Nanoscale*, 2016, **8**, 11511

Tailoring nanoarchitectonics to control the release profile of payloads†

Shuai Jiang,[a,b,c] Liping Lv,‡[a] Qifeng Li,[b] Junwei Wang,[b] Katharina Landfester[a] and Daniel Crespy*[a,d]

Received 1st February 2016,
Accepted 5th May 2016

DOI: 10.1039/c6nr00917d

www.rsc.org/nanoscale

We demonstrate here that the control over the release rate of payloads and on the selectivity of the release can be achieved by designing nanomaterials with a hierarchical structure. Redox-responsive silica nanocapsules are first synthesized to allow for an accelerated release of the corrosion inhibitor 2-mercaptobenzothiazole as a payload upon chemical reduction and retarded release upon oxidation. In a second step, we embedded the nanocapsules into nanofibers by colloid-electrospinning, yielding a hierarchical composite structure. Remarkably, the encapsulation of the nanocapsules in the fibers provides two decisive advantages that are a higher selectivity of the release and a higher control over the release rate of payloads.

Introduction

Nanomaterials are now widely investigated for the controlled release of functional payloads such as drugs,[1] corrosion inhibitors,[2,3] or self-healing agents.[4,5] One of the most important properties of nanocarriers is their release behavior, *i.e.* their ability to release selectively a payload upon one or several stimuli with a controlled release rate. Several approaches deal with the release of one payload upon several stimuli[6] or several payloads upon several stimuli.[6–8] The payload can be either entrapped physically by encapsulation in a nanocontainer,[3–6] adsorbed on the nanocarrier,[9] or chemically bonded.[7,10,11] In the latter case, a chemical reaction triggers the release of the payload either from the shell[7] or the core of the nanocarriers.[10]

Herein, we tailor nanomaterials with a hierarchical structure composed of primary objects that are stimuli-responsive inorganic nanocapsules embedded in polymer nanofibers, creating therefore multicompartment nanofibers. An immediate advantage of multicompartment nanofibers over nanocapsules is the ease of separation and re-use of such materials. Indeed, nanocapsules are usually difficult to separate from the liquid continuous phase without imparting their structural integrity whereas non-woven nanofibers can be easily separated from a surrounding liquid medium by filtration.

Up to now, the influence of a hierarchical structure of nanomaterials or nanoarchitectonics[12–15] on the release of payloads was mainly studied for mesoporous silica nanoparticles displaying stimuli-responsive gatekeeping[16,17] or porous metal–organic frameworks.[18] Significant differences in the release behavior of ibuprofen from mesoporous silica was ascribed to pore connectivity and pore geometry of the materials.[19] Another way to create hierarchical nanostructures is to embed nanomaterials in other nanomaterials. This can be efficiently realized by the colloid-electrospinning method,[20–22] in which a dispersion of polymer or inorganic nanoparticles[23,24] is electrospun with a solution of a polymer.

Stimuli-responsive metal and metal oxide nanoparticles have already been electrospun in polymer nanofibers. Magnetic nanoparticles, for example a mixture of magnetite (Fe_3O_4) and maghemite (γ-Fe_2O_3) nanoparticles, can respond to 'on–off' switching of an alternating magnetic field and generate heat. The heat induced deswelling of crosslinked thermoresponsive nanofibers composed of a copolymer of *N*-isopropylacrylamide and *N*-hydroxymethylacrylamide.[25] Thereby a controlled 'on–off' release of doxorubicin from the nanofibers was realized in response to the swelling ratio of nanofibers, which is promising for inducing cancer apoptosis.[25,26] Gold nanorods (AuNRs) can also be used because the absorption in the near-infrared region generates heat, which triggers the thermal transition of crosslinked thermoresponsive fibers. The expulsion of water from fibers upon NIR exposure facilitated the release of a protein from the fiber matrix.[27] The stimuli-responsive nanoparticles discussed above only provide a conversion of an external magnetic field or light into heat. We deal here with responsive nanocapsules

[a]*Max Planck Institute for Polymer Research, Ackermannweg 10, 55128 Mainz, Germany. E-mail: crespy@mpip-mainz.mpg.de*
[b]*Institute of Coal Chemistry, Chinese Academy of Sciences, Taiyuan 030001, China*
[c]*University of Chinese Academy of Sciences, Beijing 100049, China*
[d]*Department of Materials Science and Engineering, School of Molecular Science and Engineering, Vidyasirimedhi Institute of Science and Technology (VISTEC), Rayong 21210, Thailand*

† Electronic supplementary information (ESI) available. See DOI: 10.1039/c6nr00917d

‡ Current address: Department of Chemical Engineering, School of Environmental and Chemical Engineering, Shanghai University, Shangda Road 99, 200444, Shanghai, P. R. China.

Open Access Article. Published on 06 May 2016. Downloaded on 12/5/2025 12:51:01 PM.
This article is licensed under a Creative Commons Attribution 3.0 Unported Licence.

with high storage capacity and controlled release of functional payloads in response to changes of the surrounding environment. By embedding nanocapsules in electrospun nanofibers, an extra protection and enhanced control of the release of payloads can be realized.

To verify the applicability of our nanostructured system for the controlled release of payloads, we selected 2-mercaptobenzothiazole (MBT) as a functional payload because it is widely used as a corrosion inhibitor.[7,28,29]

Such corrosion inhibitors or self-healing agents were already encapsulated in nanocontainers.[3–5,7,10,30–32] When the nanocontainers are embedded in a coating on a metal, they can provide a sufficient barrier against a corrosive environment as well as a controlled release of corrosion inhibitors on demand. The synthesized nanocontainers are redox-responsive so that they can be activated upon onset of corrosion. The release of MBT from the responsive nanocontainers and nanocontainers in nanofibers is investigated and compared.

Experimental

Materials

Tetraethoxysilane (TEOS, Alfa Aesar, 98%), bis[3-(triethoxysilyl) propyl] tetrasulfide (TESPT, Sigma Aldrich, 90%), hexadecane (HD, Sigma Aldrich, 99%), *m*-xylene (Acros Organics, ≥99%), 2-mercaptobenzothiazole (MBT, Sigma Aldrich, 97%), cetyltrimethylammonium chloride (CTMA-Cl, Acros Organics, 99%), glutaraldehyde (GA, Merck KGaA, 50% aqueous solution), and tris(2-carboxyethyl)phosphine hydrochloride (TCEP·HCl, Alfa Aesar, ≥98%) were used as received. Polyvinyl alcohol (PVA, Polysciences Inc., 88 mol% hydrolyzed) with a molecular weight M_w of 125 000 g mol^{-1} was used as received. Distilled water was used through all the experiments if not specifically mentioned.

Encapsulation of corrosion inhibitor in the redox-responsive silica nanocapsules

Redox-responsive silica nanocapsules loaded with corrosion inhibitors were synthesized by miniemulsion polymerization similarly to a previous procedure as shown in Fig. 1a.[33,34] The surface of miniemulsion droplets was used as a soft template for the hydrolysis and condensation of silicon alkoxides. Alkoxysilane precursors (1.5 g of TEOS and 0.5 g of TESPT) were first mixed with 125 mg of HD, 1 g of *m*-xylene, and 25 mg of MBT, and then added to 30 mL of a 0.77 mg mL^{-1} aqueous solution of CTMA-Cl. After pre-emulsification under 1000 rpm for 1 h at room temperature, the emulsion was sonicated with ice cooling for 180 s at 70% amplitude in a pulse regime (30 s sonication, 10 s pause) using a Branson 450 W sonifier and a 1/2″ tip. The resulting miniemulsions were stirred under 1000 rpm at room temperature overnight to obtain the silica nanocapsules.

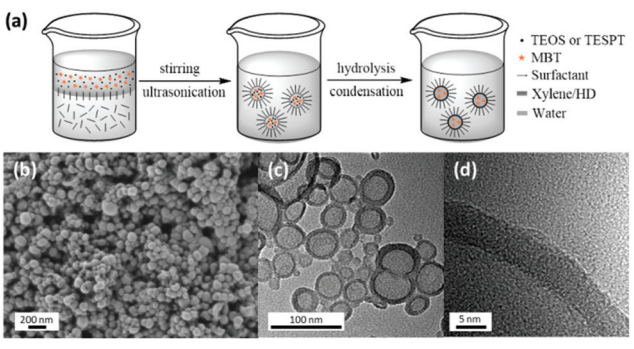

Fig. 1 (a) Schematic illustration of the formation of redox-responsive silica nanocapsules using miniemulsion polymerization; (b) SEM and (c) TEM micrographs of the responsive silica nanocapsules; (d) high-resolution TEM micrograph of the shell of silica nanocapsules.

Preparation of redox-responsive multicompartment nanofibers by colloid-electrospinning

The fibers were obtained through electrospinning an aqueous solution of PVA mixed with an aqueous dispersion of silica nanocapsules. Firstly, 15 wt% PVA aqueous solution was prepared by dissolving PVA in distilled water at 80 °C with vigorous stirring for 2 h. The electrospinning solution was prepared by mixing the 15 wt% PVA solution with dispersions of silica nanocapsules with a weight ratio of 2.75 : 2.25. Electrospinning was carried out using a model fabricated by IME Technologies with an applied voltage of 15 kV, a distance between the spinneret and the collector of 10 cm, and a feeding rate of 0.2 mL h^{-1}. For the SEM and TEM samples, the collecting time was 10 s; while the collecting time was 12 h for the study of the release of the payloads. The diameter of electrospun nanofibers was estimated by counting at least 100 nanofibers from SEM micrographs.

Crosslinking of the fiber matrix

The electrospun nanofibrous mats were crosslinked by exposure to glutaraldehyde (GA)/HCl vapor in a vacuum desiccator for 1 h. 1 mL of 50 wt% GA aqueous solution and 20 μL of 37 wt% HCl aqueous solution were used as sources of GA and HCl vapor, respectively. HCl serves as the catalyst for the reaction between the hydroxyl groups of PVA chains and aldehyde groups of GA to form acetal bridges.[35] Afterwards, the crosslinked nanofibrous mat was exposed to air flow in the hood for 24 h before use in order to evaporate the unreacted GA and HCl.

Redox-responsive release of MBT from silica nanocapsules and nanofibers

To study the redox-responsive release of MBT from silica nanocapsules, 0.1 mL of the dispersions of silica nanocapsules and 0.9 mL of distilled water were placed into a dialysis bag (MWCO 14 000) with both ends sealed. After that, the dialysis bag was immersed into 9 mL of aqueous dialysis medium with 0, 0.07, 0.7, or 7 mmol L^{-1} TCEP·HCl (corresponding to molar ratios TCEP : TESPT = 0 : 1, 0.3 : 1, 3 : 1, 30 : 1) with a magnetic stirring rate (300 rpm), at room temperature. For the reduction–oxidation–reduction study, 10 mL of 0.07 mmol L^{-1} TCEP·HCl was used to create the initial reducing environment. After 30 min, 0.4 mL of 7 mmol L^{-1} aqueous solution of H_2O_2

 This journal is © The Royal Society of Chemistry 2016

Open Access Article. Published on 06 May 2016. Downloaded on 12/5/2025 12:51:01 PM.
This article is licensed under a Creative Commons Attribution 3.0 Unported Licence.

was added to create an oxidizing environment. 1 h later, 0.2 mL of 7 mmol L^{-1} aqueous solution of TCEP·HCl and 0.2 mL distilled water were added again to restore the initial reducing environment. In the case of redox-responsivity studies of the nanofibers, 24 mg of nanofibrous mats (containing the same amount of MBT as in the nanocapsules system) and 1.0 mL of distilled water were placed into a dialysis bag that was immersed into 9 mL of an aqueous dialysis medium composed of 0, 0.07, 0.7, or 7 mmol L^{-1} aqueous solutions of TCEP·HCl. The following procedures are the same for the dispersion of the nanocapsules and the nanofibers. After given time intervals, 0.4 mL of the solution outside the dialysis bag was taken out for UV-Vis measurements. An equal amount of fresh solution was added to maintain the concentration of the redox agent constant. The concentration of released MBT was determined by monitoring the absorption of the peak $\lambda_{max} \sim$ 311 nm by using UV-Vis spectroscopy. A calibration curve drawn by measuring a series of MBT solutions with known concentrations in our previous work was used.[7]

Characterization

The hydrodynamic diameter of silica nanocapsules was evaluated by dynamic light scattering (DLS) using a Nicomp particle sizer (Model 380, PSS, Santa Barbara, CA) at a fixed scattering angle of 90°. The shell thickness of the obtained nanocapsules was estimated by counting at least 100 capsules from TEM micrographs. The morphologies of silica nanocapsules and nanofibers were examined with a Gemini 1530 (Carl Zeiss AG, Oberkochem, Germany) scanning electron microscope (SEM) operating at 0.35 kV and a Jeol 1400 (Jeol Ltd, Tokyo, Japan) transmission electron microscope (TEM) operating at an accelerating voltage of 120 kV. SEM and TEM samples of silica nanocapsules were prepared by casting the diluted nanocapsule dispersions on silicon wafers and 400-mesh carbon layer-coated copper grids, respectively. The samples of nanofibers for SEM and TEM were prepared by depositing electrospun nanofibers on silicon wafers and copper grids, respectively. The UV-Vis absorption spectra of MBT solution were recorded with a Perkin Elmer Lambda 25 UV-Vis spectrometer. The surface area of the silica nanocapsules was determined from nitrogen adsorption–desorption experiments by using a Quantachrome Autosorb-1 analyzer (Boynton Beach, FL) at 77.3 K. The capsule dispersions were dialyzed in demineralized water for 3 days to remove the surfactant and then freeze-dried for 48 h and degassed at 70 °C for 12 h under high vacuum before measurements. The specific surface area was calculated using the Brunauer–Emmett–Teller (BET) equation based on data points obtained from $0 < P/P_0 < 0.25$. The encapsulation efficiency of MBT in silica nanocapsules was estimated by using UV-vis spectroscopy. 0.5 mL of the miniemulsion was first mixed with 0.5 mL of 35 g L^{-1} NaCl solution to destabilize the capsule dispersion. The mixture was centrifuged at 4000 rpm to separate the capsules from the dispersion. The supernatant was analyzed by using UV-vis spectroscopy according to a preliminary calibration at ~311 nm and compared to the theoretical loading amount.

Results and discussion

Encapsulation of corrosion inhibitor in the redox-responsive silica nanocapsules

The corrosion inhibitor 2-mercaptobenzothiazole (MBT) was encapsulated in the redox-responsive silica nanocapsules by using a hydrolysis and condensation reaction of tetraethoxysilane (TEOS) and bis[3-(triethoxysilyl)propyl] tetrasulfide (TESPT) at the interface of miniemulsion droplets. A certain amount of MBT, 0.8 wt% compared to the dispersed phase, was first dissolved in the dispersed phase and then encapsulated in the liquid core of the nanocontainers for 12 h. The loading efficiency of MBT in the capsules was calculated to be 96% by UV-vis spectroscopy. TESPT was introduced as redox-responsive units in the silica shell in order to yield a redox-responsive permeability behavior. The well-defined core–shell morphology of silica nanocapsules was identified by SEM and TEM as shown in Fig. 1b–d, which indicated the successful condensation of the alkoxysilanols at the interface of the miniemulsion droplets. The obtained capsules exhibited a number-average hydrodynamic diameter of 248 ± 135 nm and a shell thickness of 6 ± 1 nm (as determined by TEM images), close to the theoretical value of 7.6 nm determined by calculating the thickness assuming 100% conversion, a density of silica equal to the bulk, and taking the number weighted average hydrodynamic diameter as the diameter of the capsules.

Redox-responsive release of MBT from silica nanocapsules

Three redox conditions (control, reduction, and oxidation) were studied to simulate different electrochemical potentials during the corrosion process (Fig. 2a): no potential application simulating intact coating, low potential simulating the onset of corrosion, and high potential simulating the passivation of the metal.[3] The redox-responsive property of the silica nanocapsules was first investigated with different concentrations of the reducing agent (see Fig. 2b). Tris(2-carboxyethyl)phosphine hydrochloride (TCEP·HCl) was selected here as a water-soluble reducing agent because it is highly effective for the reduction of disulfide bonds.[36] When no reducing trigger was applied, the silica capsules showed a burst release (~54%) of MBT in the first 1 h, showing therefore a relatively high percentage of non-specific release, *i.e.* a release that occurs independently under the redox conditions. This observation can be explained by the porosity of the silica shell that has a BET surface area of 141 m^2 g^{-1}, pore volume of 0.7 cm^3 g^{-1} and average pore size of 18.6 nm. The nitrogen adsorption–desorption isotherm of silica capsules exhibited a typical IV isotherm with H3 type hysteresis loops with a relative pressure P/P_0 in the range of 0.5–1.0.[37,38] The nitrogen adsorption–desorption isotherm and pore size distribution of dried capsules are shown in Fig. S1.† As the concentration of TCEP increased, the release of MBT accelerated accordingly. This acceleration was due to the reduction of tetrasulfide linkages, which lead to an increase of the permeability of the silica shell.[33] When the release equilibrium was reached, almost 100% release was observed for all concentrations of TCEP. During the corrosion process of met-

Open Access Article. Published on 06 May 2016. Downloaded on 12/5/2025 12:51:01 PM.
This article is licensed under a Creative Commons Attribution 3.0 Unported Licence.

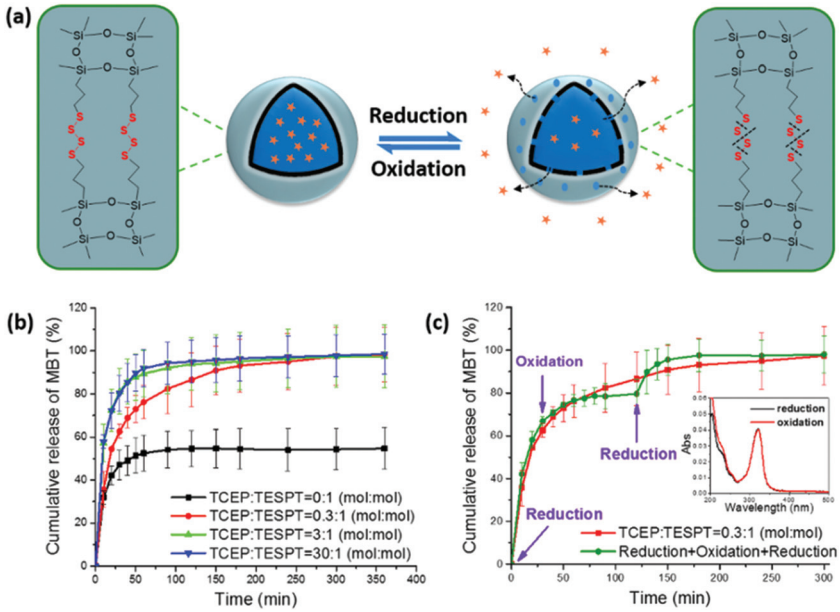

Fig. 2 (a) Scheme depicting the release mechanism of MBT from silica capsules upon reduction and oxidation; (b) release of MBT from silica nanocapsules in response to different concentrations of TCEP; (c) controlled release of MBT from silica nanocapsules upon reduction and oxidation. Inset: UV absorption of MBT upon reduction and oxidation conditions.

allic materials, the anodic metals are oxidized and release electrons which could be used for the reduction of disulfide bonds. MBT has been reported as an effective corrosion inhibitor for the protection of zinc.[39] Zinc has a standard electrode potential of −0.76 V,[40] which is lower than the standard redox potential of disulfide bonds (−0.25 mV).[41] Therefore, the disulfide linkages in the capsule shell could be cleaved during the corrosion process, thereby increase the shell permeability and promote the release of MBT to stop the corrosion. The electrochemical reduction was also proved to be useful for the cleavage of the stable cyclic disulfides to the corresponding dithiols.[42]

To further investigate the redox-responsive properties, silica nanocapsules were treated in a sequential reduction–oxidation–reduction (see Fig. 2c). Silica nanocapsules were first placed in a reducing environment (TCEP : TESPT = 0.3 : 1 mol : mol). A fast release (~68%) of MBT was observed in the first 30 min. The capsules were opened and released the loaded inhibitors after their reduction. After 30 min, an oxidizing environment was created by adding the double molar amount of H_2O_2 compared to the molar amount of TCEP added to the system. As expected, the release of MBT was found to be hindered as a consequence of the combined effect of both re-connecting the tetrasulfide bridges by oxidation and the bonding of MBT with the thiol group from the cleaved tetrasulfide bonds. Because the initial molar ratio of TCEP and tetrasulfide bonds was 0.3 : 1, only 30% of tetrasulfide linkages in the shell of the capsules were theoretically reduced. Ideally, the capsules could detect the rise of electrochemical potential as soon as the corrosive attack ends, and then reseal the capsule wall and stop the release of inhibitor automatically. The influence of redox potential on the UV absorption of MBT can be excluded based on the fact that there was no obvious difference between the absorption of MBT under reducing and oxidizing conditions (see the inset of Fig. 2c). When chemical reduction was applied again, a ~100% release of loaded MBT was observed in 1 h. This phenomenon indicated the reversibility and control of the redox-responsive property of the silica nanocapsules. The morphologies of silica nanocapsules after release are shown in Fig. 5a–c. The capsules after reduction and oxidation remained intact. No collapse of capsules was observed which verified the good mechanical integrity of silica capsules after release of the payloads.

Preparation of multicompartment nanofibers by colloid-electrospinning

The materials with the hierarchical structure nanocapsules in nanofibers were prepared by the colloid-electrospinning technique. When a strong electrical field is applied to the dispersion, the droplet at the tip of the needle experiences a conical deformation (Taylor cone). Once the electrostatic force overcomes the surface tension of the droplets, the dispersion is ejected towards the collector in the form of a jet. The solvent evaporates on the way to the collector and nanofibers are deposited on the collector as non-woven fibers (Fig. 3a).[20] The silica nanocapsules were found to be well distributed in the nanofibers as indicated by SEM and TEM (see Fig. 3b and c). Remarkably, the core–shell structure of the nanocapsules can be still recognized after being embedded in the nanofibers (Fig. 3c). The diameter of fibers was estimated to be 200 ± 50 nm.

 This journal is © The Royal Society of Chemistry 2016

Open Access Article. Published on 06 May 2016. Downloaded on 12/5/2025 12:51:01 PM.
This article is licensed under a Creative Commons Attribution 3.0 Unported Licence.

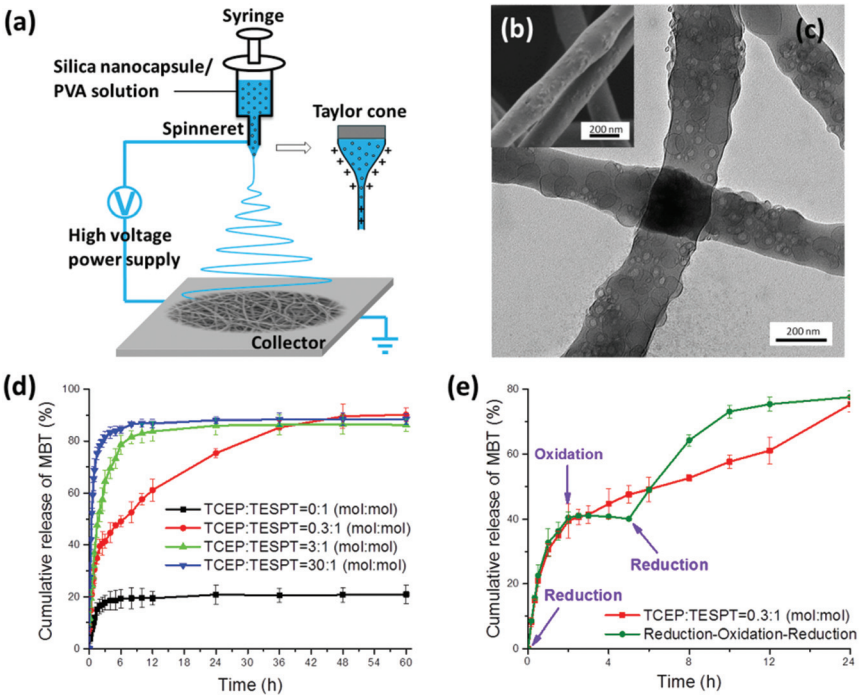

Fig. 3 (a) Schematic illustration of the formation of the nanocapsules-in-nanofiber structures by the colloid-electrospinning technique; (b) SEM and (c) TEM micrographs of the fibers; (d) release of MBT from the nanofibers in response to different concentrations of TCEP; (e) controlled release of MBT from the nanofibers upon reduction and oxidation.

The advantage of this multicompartment structure over the more conventional core-sheath fiber structure is that it allows for a local release since the multicompartments are discontinuous. In a continuous core-sheath fiber structure, all the payloads would be released upon activation with a stimulus or by mechanical damage. The second advantage is that in principle several types of nanocontainers can be embedded that are activated upon different stimuli. Electrospun nanofibers were rendered water-stable by crosslinking them in glutaraldehyde and HCl vapor. Since no organic solvent was used, the release of loaded inhibitors during the crosslinking process could be avoided. The immediate advantage of such nanocapsules-in-nanofibers materials is that they can be easily separated from a liquid surrounding medium, which is not always easy for a dispersion of nanocapsules.

Redox-responsive release of MBT from multicompartment nanofibers

The redox-responsive property of silica nanocapsules after their embedding in electrospun nanofibers was studied and compared with the one displayed by the nanocapsules in dispersion (Fig. 3d and e). The nanofibers were found to be also redox-responsive, meaning that the functionality of the silica capsules can be activated even after being embedded in the nanofibers. Two main differences were observed. First of all, the release of MBT from the nanofibers was much slower than the release from the nanocapsules. That observation is true for all ratios TCEP : TESPT and particularly marked for the ratio TCEP : TESPT = 0.3 : 1, for which the duration for the release of 80% of the initial quantity of the payload is 23 times higher than that for nanocapsules (Fig. 4a). This means that burst release from nanocapsules can be avoided if they are embedded in nanofibers. This hindrance of burst release is attributed to the barrier effect of the polymer matrix forming the nanofibers, yielding longer pathways for the molecules involved in the chemical stimulus and the molecules of the payloads. Although still high (80–90%), the absolute released amount of payloads was lower in the case of the nanocapsules-in-nanofibers. We cannot exclude that part of the MBT could have reacted with the residual aldehyde groups of GA bonded to PVA chains during the crosslinking process to yield a hemithioacetal.[43] The morphologies of the fibers after crosslinking

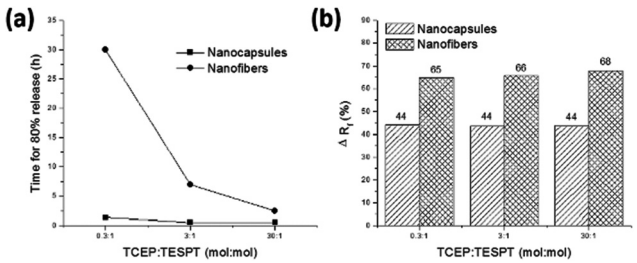

Fig. 4 (a) Time for 80% release of MBT from nanocapsules and nanofibers upon different molar ratios of TCEP and TESPT; (b) selectivity of the release of MBT from nanocapsules and nanofibers upon different molar ratios of TCEP and TESPT.

Open Access Article. Published on 06 May 2016. Downloaded on 12/5/2025 12:51:01 PM.
This article is licensed under a Creative Commons Attribution 3.0 Unported Licence.

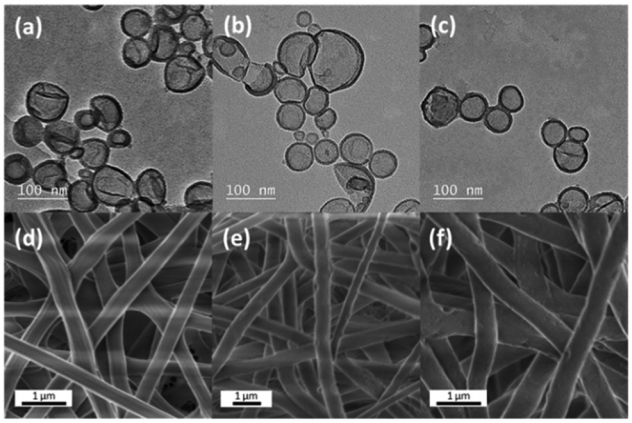

Fig. 5 TEM micrographs of silica nanocapsules under different conditions: (a) control (in water), (b) reduction (TCEP : TESPT = 30 : 1 mol : mol), and (c) reduction–oxidation–reduction; SEM micrographs of nanofibers: (d) after cross-linking, (e) after release in water and (f) after release under reduction (TCEP : TESPT = 30 : 1 mol : mol).

and release of the payloads were intact as shown in Fig. 5d–f. The capsules can be still identified in the fibers by TEM (see Fig. S2†).

The second main difference and advantage of the hierarchical structure is the increase of selectivity. We defined the selectivity $\Delta R_f = R_f\,(S) - R_f\,(NS)$ with $R_f\,(S)$ and $R_f\,(NS)$ being the final % release for the samples stimulus-activated and the final % release for the samples that are not activated by the chemical stimulus, respectively. This value gives therefore a relative quantity reflecting the selectivity of the release system – the part of the performance in the release that is dependent only on the redox-responsive property of the system. The selectivity of the nanofiber constructs was found to be always higher than for the nanocapsules (Fig. 4b), the average difference being ~20%.

Conclusions

Materials with hierarchical structures consisting of nanocapsules-in-nanofibers were synthesized by colloid-electrospinning. The redox-responsive properties of the nanocapsules could be conserved when they were in the fibers and therefore both dispersion of nanocapsules and nanocapsules-in-nanofibers could release a corrosion inhibitor selected as a payload upon chemical reduction of the nanocapsules. The hierarchical structures showed three main beneficial features. The first one is the ease of separation of nanofibrous structures by filtration compared to nanocapsules. A second remarkable advantage is that burst release is prevented and that the release of the corrosion inhibitor can be prolonged by a factor of more than 20 times. Finally, the selectivity of the release is increased by ~20% compared to the release from nanocapsules. Therefore, the nanocapsules-in-nanofibers are promising constructs for the controlled release of payloads. In view of the change of redox potential during the corrosion process[3] and the potential difference between the extra- and intracellular environment,[44] the present concept is promising for the application of corrosion protection and drug delivery.

Acknowledgements

We acknowledge the financial support from "MPG-CAS Joint Doctoral Promotion Program (DPP)".

Notes and references

1 D. A. Lavan, T. McGuire and R. Langer, *Nat. Biotechnol.*, 2003, **21**, 1184.
2 D. Shchukin and H. Möhwald, *Science*, 2013, **341**, 1458.
3 A. Vimalanandan, L. P. Lv, T. H. Tran, K. Landfester, D. Crespy and M. Rohwerder, *Adv. Mater.*, 2013, **25**, 6980.
4 B. Blaiszik, N. Sottos and S. White, *Compos. Sci. Technol.*, 2008, **68**, 978.
5 J. Fickert, M. Makowski, M. Kappl, K. Landfester and D. Crespy, *Macromolecules*, 2012, **45**, 6324.
6 R. H. Staff, M. Gallei, K. Landfester and D. Crespy, *Macromolecules*, 2014, **47**, 4876.
7 L.-P. Lv, K. Landfester and D. Crespy, *Chem. Mater.*, 2014, **26**, 3351.
8 W. Xu, A. A. Steinschulte, F. A. Plamper, V. F. Korolovych and V. V. Tsukruk, *Chem. Mater.*, 2016, 975.
9 M. S. Yavuz, Y. Cheng, J. Chen, C. M. Cobley, Q. Zhang, M. Rycenga, J. Xie, C. Kim, K. H. Song and A. G. Schwartz, *Nat. Mater.*, 2009, **8**, 935.
10 L.-P. Lv, Y. Zhao, K. Landfester and D. Crespy, *Polym. Chem.*, 2015, **6**, 5596.
11 S. Dhar, N. Kolishetti, S. J. Lippard and O. C. Farokhzad, *Proc. Natl. Acad. Sci. U. S. A.*, 2011, **108**, 1850.
12 M. Aono, Y. Bando and K. Ariga, *Adv. Mater.*, 2012, **24**, 150.
13 K. Ariga, Q. Ji, W. Nakanishi, J. P. Hill and M. Aono, *Materi. Horiz.*, 2015, **2**, 406.
14 M. Aono and K. Ariga, *Adv. Mater.*, 2015, 989.
15 K. Ariga, J. Li, J. Fei, Q. Ji and J. P. Hill, *Adv. Mater.*, 2015, 1251.
16 I. I. Slowing, J. L. Vivero-Escoto, C.-W. Wu and V. S.-Y. Lin, *Adv. Drug Delivery Rev.*, 2008, **60**, 1278.
17 M. Vallet-Regí, F. Balas and D. Arcos, *Angew. Chem., Int. Ed.*, 2007, **46**, 7548.
18 P. Horcajada, T. Chalati, C. Serre, B. Gillet, C. Sebrie, T. Baati, J. F. Eubank, D. Heurtaux, P. Clayette and C. Kreuz, *Nat. Mater.*, 2010, **9**, 172.
19 J. Andersson, J. Rosenholm, S. Areva and M. Lindén, *Chem. Mater.*, 2004, **16**, 4160.
20 D. Crespy, K. Friedemann and A. M. Popa, *Macromol. Rapid Commun.*, 2012, **33**, 1978.
21 C.-L. Zhang and S.-H. Yu, *Chem. Soc. Rev.*, 2014, **43**, 4423.
22 M. Beck-Broichsitter, M. Thieme, J. Nguyen, T. Schmehl, T. Gessler, W. Seeger, S. Agarwal, A. Greiner and T. Kissel, *Macromol. Biosci.*, 2010, **10**, 1527.

This journal is © The Royal Society of Chemistry 2016

Open Access Article. Published on 06 May 2016. Downloaded on 12/5/2025 12:51:01 PM.
This article is licensed under a Creative Commons Attribution 3.0 Unported Licence.

23 K. Friedemann, T. Corrales, M. Kappl, K. Landfester and D. Crespy, *Small*, 2012, **8**, 144.
24 C. Wu, W. Yuan, S. S. Al-Deyab and K.-Q. Zhang, *Appl. Surf. Sci.*, 2014, **313**, 389.
25 Y. J. Kim, M. Ebara and T. Aoyagi, *Adv. Funct. Mater.*, 2013, **23**, 5753.
26 S.-R. Huang, K.-F. Lin, C.-F. Lee and W.-Y. Chiu, *J. Polym. Sci., Part A: Polym. Chem.*, 2014, **52**, 848.
27 V. V. Ramanan, K. C. Hribar, J. S. Katz and J. A. Burdick, *Nanotechnology*, 2011, **22**, 494009.
28 F. Maia, J. Tedim, A. D. Lisenkov, A. N. Salak, M. L. Zheludkevich and M. G. Ferreira, *Nanoscale*, 2012, **4**, 1287.
29 M. Ohsawa and W. Suëtaka, *Corros. Sci.*, 1979, **19**, 709.
30 Y. Zhao, J. Fickert, K. Landfester and D. Crespy, *Small*, 2012, **8**, 2954.
31 M. Huang and J. Yang, *J. Mater. Chem.*, 2011, **21**, 11123.
32 D. G. Shchukin, M. Zheludkevich, K. Yasakau, S. Lamaka, M. G. Ferreira and H. Moehwald, *Adv. Mater.*, 2006, **18**, 1672.
33 J. Fickert, D. Schaeffel, K. Koynov, K. Landfester and D. Crespy, *Colloid Polym. Sci.*, 2014, **292**, 251.
34 J. Fickert, P. Rupper, R. Graf, K. Landfester and D. Crespy, *J. Mater. Chem.*, 2012, **22**, 2286.
35 H. S. Mansur, C. M. Sadahira, A. N. Souza and A. A. P. Mansur, *Mater. Sci. Eng. C*, 2008, **28**, 539.
36 J. A. Burns, J. C. Butler, J. Moran and G. M. Whitesides, *J. Org. Chem.*, 1991, **56**, 2648.
37 Y. Wang, T. Su, H. Chen, W. Liu, Y. Dong and S. Hu, *Mater. Lett.*, 2014, **137**, 241.
38 Y. J. Kim, X. Xing, D.-Y. Choi, C.-H. Hwang, C. Choi, G. Kim, S. Jin, K.-J. Hwang and J.-Y. Park, *New J. Chem.*, 2015, **39**, 7754.
39 H. Yang, Y. Sun, J. Ji, W. Song, X. Zhu, Y. Yao and Z. Zhang, *Corros. Sci.*, 2008, **50**, 3160.
40 G. H. Kim, W. H. Jeong, B. Du Ahn, H. S. Shin, H. J. Kim, H. J. Kim, M.-K. Ryu, K.-B. Park, J.-B. Seon and S.-Y. Lee, *Appl. Phys. Lett.*, 2010, **96**, 163506.
41 S. W. Ragsdale and Y. Li, *Antioxid. Redox Signaling*, 2011, **14**, 1039.
42 Z. E. Shaked, J. J. Barber and G. M. Whitesides, *J. Org. Chem.*, 1981, **46**, 4100.
43 A. G. Destaye, C.-K. Lin and C.-K. Lee, *ACS Appl. Mater. Interfaces*, 2013, **5**, 4745.
44 G. Saito, J. A. Swanson and K.-D. Lee, *Adv. Drug Delivery Rev.*, 2003, **55**, 199.